NANO · MICRO small
www.small-journal.com

Birefringence and Dichroism in Quasi-1D Transition Metal Trichalcogenides: Direct Experimental Investigation

Shijun Hou, Zhengfeng Guo, Juehan Yang, Yue-Yang Liu, Wanfu Shen, Chunguang Hu, Shiyuan Liu, Honggang Gu, and Zhongming Wei**

Birefringence and dichroism are very important properties in optical anisotropy. Understanding the intrinsic birefringence and dichroism of a material can provide great help to utilize its optical anisotropy. But the direct experimental investigation of birefringence in nanoscale materials is rarely reported. As typical anisotropic transition metals trichalcogenides (TMTCs) materials with quasi-1D structure, TiS_3 and ZrS_3 have attracted extensive attention due to their special crystal structure and optical anisotropy characteristics. Here, the optical anisotropy properties such as birefringence and dichroism of two kinds of quasi-1D TMTCs, TiS_3 and ZrS_3, are theoretically and experimentally studied. In experimental results, the anisotropic refraction and anisotropic reflection of TiS_3 and ZrS_3 are studied by polarization-resolved optical microscopy and azimuth-dependent reflectance difference microscopy, respectively. In addition, the birefringence and dichroism of ZrS_3 nanoribbon in experiment are directly measured by spectrometric ellipsometry measurements, and a reasonable result is obtained. This work provides the basic optical anisotropy information of TiS_3 and ZrS_3. It lays a foundation for the further study of the optical anisotropy of these two materials and provides a feasible method for the study of birefringence and dichroism of other nanomaterials in the future.

1. Introduction

For optical research, optical anisotropy is a very important topic and attracting more attention. At present, the polarizer, waveplate and other optical devices closely related to optical anisotropy.[1–5] The degree of optical anisotropy of a material is determined by the real and imaginary parts of the complex refractive indices along different axes of the material and can be further described as the birefringence and dichroism of the material.[6] Among all kinds of optical anisotropic materials, transition metals trichalcogenides (TMTC) materials have attracted more attention due to their unique crystal structure, optical properties and electrical properties.[7–15] Among the numerous TMTC materials, there is a material system MS_3 (M = Ti, Zr, Hf) the transition metal element as the IVB group element, and the ratio of transition metal element to sulfur element is 1:3. MS_3 bulk materials are wire-like crystals, and the mono-layered materials obtained by mechanically separated are nanoribbons with quasi-1D structure. Previous studies have shown that MS_3 has strong in-plane optical anisotropy properties, which is caused by the difference of crystal structure along different directions in-plane.[15,16] MS_3 is considered to have great potential in application of optical and electronic devices because of its unique quasi-1D crystal structure and strong optical anisotropy.[11,17–22]

Previous studies have shown that the dichroic ratio of TiS_3 is 4:1[16] and that of ZrS_3 is 2.55:1.[15] The best excitation energy of the dichromatic ratio generated by photocurrent was 1.00–2.0 eV for TiS_3 and 2.0 to 3.0 eV for ZrS_3.[23] The optical anisotropies of TiS_3 and ZrS_3 quasi-1D materials were studied systematically by both theory and experiments, including the optical absorption, reflection, refractive index and extinction coefficient. We studied the reflection and refraction of quasi-1D TiS_3 and ZrS_3 by using polarization-resolved optical microscopy (PROM) and azimuth-dependent reflectance difference microscopy (ADRDM). In addition, we first measured the anisotropic refractive indices and extinction coefficients of ZrS_3 in experimental by spectrometric ellipsometry (SE) measurements, and then compared and analyzed the results obtained by theoretical

S. Hou, Dr. J. Yang, Dr. Y.-Y. Liu, Prof. Z. Wei
State Key Laboratory of Superlattices and Microstructures
Institute of Semiconductors
Chinese Academy of Sciences & Center of Materials Science and Optoelectronics Engineering
University of Chinese Academy of Sciences
Beijing 100083, China
E-mail: zmwei@semi.ac.cn

Z. Guo, Prof. S. Liu, Dr. H. Gu
State Key Laboratory of Digital Manufacturing Equipment and Technology
Huazhong University of Science and Technology
Wuhan 430074, China
E-mail: hongganggu@hust.edu.cn

Dr. W. Shen, Prof. C. Hu
State Key Laboratory of Precision Measuring Technology and Instruments
Tianjin University
Tianjin 300072, China

The ORCID identification number(s) for the author(s) of this article can be found under https://doi.org/10.1002/smll.202100457.

DOI: 10.1002/smll.202100457

calculation. This work may contribute to the application and development of optoelectronic anisotropy devices based on quasi-1D TMTC materials.

2. Results and Discussion

2.1. Crystal Structure and Density Functional Theory Calculations

Both TiS_3 and ZrS_3 are TMTCs, the metal elements belong to IVB group, and the ratio of metal elements to sulfur is 1:3. More importantly, both of two materials are monoclinic and their lattice constants are a = 4.958 Å, b = 3.401 Å, and c = 8.778 Å for TiS_3 and a = 5.124 Å, b = 3.624 Å, and c = 8.980 Å for ZrS_3.[24] Their crystal structures are drawn by VESTA[25] and shown in Figure S1a, Supporting Information, and **Figure 1**a. It is obvious that the two materials have very similar crystal structures. In the plane, the direction along a-axis is armchair direction, and the direction along b-axis is zigzag direction, with obvious anisotropic structure. Both TiS_3 and ZrS_3 layers are stacked by van der Waals forces along the c-axis. Because the van der Waals force is a weak interaction force, the two materials can be mechanically separated to obtain a few layered quasi-1D nanoribbons, which enables us to better study their optical anisotropy from the low-dimensional structure. The special in-plane structure of such TMTC materials that lead to their strong optical anisotropy.

In order to investigate the optical anisotropy of TiS_3 and ZrS_3 deeply, we used Heyd–Scuseria–Ernzerhof (HSE06) methods[26] to calculate the band structure, transition dipole moment and anisotropy optical absorption of TiS_3 and ZrS_3. Both TiS_3 and ZrS_3 we calculated are bulk materials. The band structure and transition dipole moment of TiS_3 are shown in Figure S1b, Supporting Information. Bulk TiS_3 has indirect band gap structure with E_g = 0.97 eV and this result is in a good agreement with previous work.[27] As for ZrS_3, the calculation results are shown in Figure 1b. The results shows that bulk ZrS_3 also has indirect band gap structure with E_g = 1.96 eV. The electron transition occurs at the band position corresponding to the maximum peak of the transition dipole moment. Calculated partial charge density (PCD) of valence band maximum (VBM) and conduction band minimum (CBM) in TiS_3 and ZrS_3 are drawn by VESTA[25] and shown in Figure S1c,d, Supporting Information, and Figure 1c,d. In addition, we also calculated the optical absorption of TiS_3 and ZrS_3 along a-axis and b-axis, respectively, and the calculated results are shown in Figure S1e, Supporting Information, and Figure 1e. For both two materials, significant differences in optical absorption along the armchair direction (a-axis direction) and the zigzag direction (b-axis direction) can be found. The absorption edge of TiS_3 on a-axis is greater than 600 nm, while the absorption edge for TiS_3 on b-axis is ≈500 nm. The absorption edge of a-axis for ZrS_3 is at ≈500 nm, while the absorption edge of b-axis is at ≈350 nm. This result indicates that both TiS_3 and ZrS_3 have in-plane optical anisotropy properties, which is consistent with the previous and experimental results.[13–16]

In this work, the electronic and optical properties were computed by using first-principles methods, which are programmed in Vienna ab initio simulation package.[28–31] The electron exchange-correlation is treated with generalized gradient approximation of Perdew–Burke–Ernzerhof.[32] The

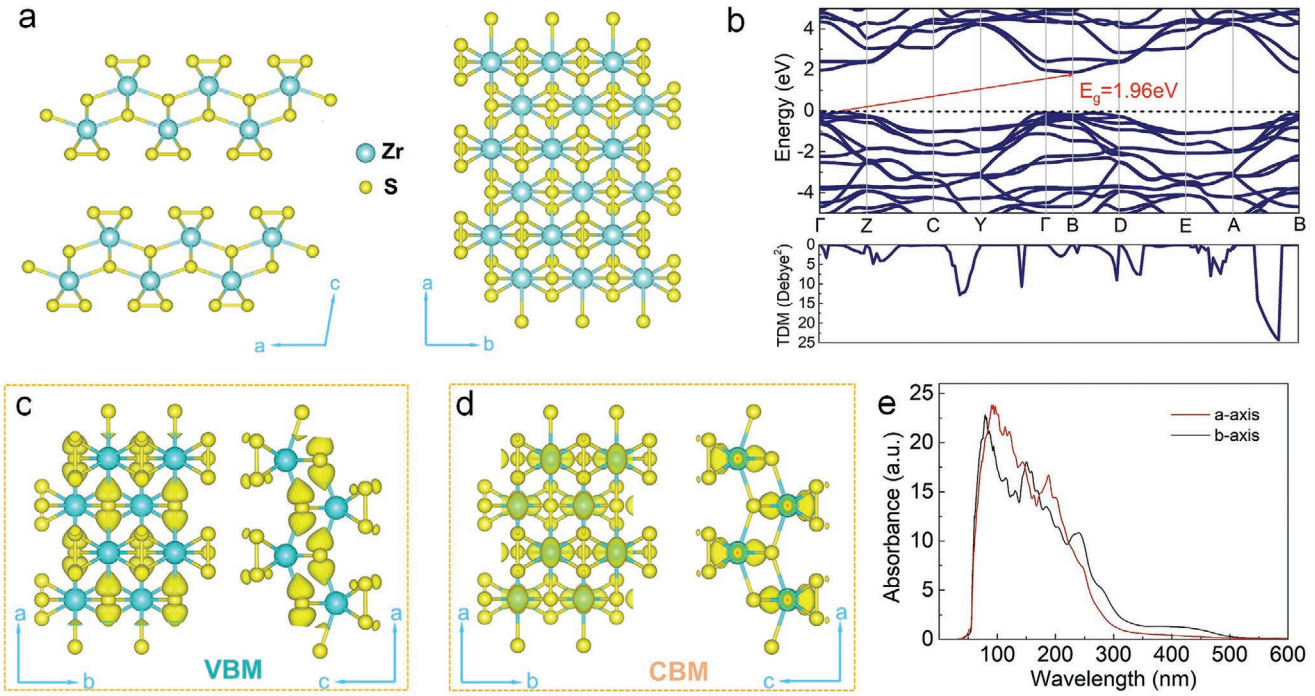

Figure 1. a) Crystal structure of ZrS_3. b) Calculated band structure and transition dipole moment of ZrS_3. c) Calculated PCD of VBM in ZrS_3. d) Calculated PCD of CBM in ZrS_3. e) Calculated anisotropy optical absorbance along the a-axis and b-axis of ZrS_3.

projected augmented wave potential with the plane wave cutoff of 500 eV is selected.[33] The Brillouin zone is integrated with k meshes of $7 \times 7 \times 3$.[34] All the calculation precision for energy and forces are 10^{-5} eV and 0.01 eV Å^{-1}, respectively. The optical absorption coefficient $\alpha(\omega)$ is calculated as:

$$\alpha(\omega) = \sqrt{2}\,\omega\left[\sqrt{\varepsilon_1^2(\omega)+\varepsilon_2^2(\omega)} - \varepsilon_1(\omega)\right]^{\frac{1}{2}} \quad (1)$$

where $\varepsilon_1(\omega)$ and $\varepsilon_2(\omega)$ are the real and imaginary parts of the complex dielectric function, respectively.

2.2. Characterization of TiS_3 and ZrS_3 Nanoribbons

In this work, TiS_3 and ZrS_3 nanoribbons are mechanical exfoliated from bulk materials, and characterized by transmission electron microscopy (TEM). A high-resolution TEM (HRTEM) image of TiS_3 is shown in **Figure 2**a. In the figure, the planes spacing along different directions is 0.50 and 0.34 nm, which is consistent with the distance of {100} and {010} lattice planes, respectively. The high crystallinity and crystal orientation of TiS_3 crystals are represented by the selected-area electron diffraction (SAED) pattern, as shown in Figure 2b. Figure 2c shows an optical image and low-magnification TEM image of TiS_3 nanoribbon. The clear shape of TiS_3 nanoribbon is exhibited in those two images. Furthermore, Figure 2c also points out the distribution of S elements and Ti elements in TiS_3 nanoribbons. It can be clearly observed that S elements and Ti elements are uniformly distributed in TiS_3 nanoribbons.

For ZrS_3, the characterization method is the same as for TiS_3, and Figure 2d–f shows the results. Figure 2d shows the HRTEM image of ZrS_3. In the figure, the planes spacing along different directions are 0.51 and 0.36 nm, which is consistent with the distance of {100} and {010} lattice planes, respectively. Figure 2e shows the high crystallinity and crystal orientation of ZrS_3 crystal in SAED pattern image. An optical image and low-magnification TEM image of ZrS_3 nanoribbon are shown in Figure 2f. Those two images exhibit the clear shape of ZrS_3 nanoribbon. Otherwise, Figure 2f also gives the distribution of S elements and Zr elements in ZrS_3 nanoribbons. It is clear that S elements and Zr elements are uniformly distributed in ZrS_3 nanoribbons, the same as TiS_3.

2.3. Optical Anisotropy Reflection and Visualized Birefringence

In order to further investigate the optical anisotropy of TiS_3 and ZrS_3 experimentally, the anisotropy reflection and visualized birefringence of the two materials were investigated by using the ADRDM and PROM. ADRDM has been widely used in the optical study of in-plane anisotropy reflection of many 2D materials.[35] For ADRDM test, TiS_3 and ZrS_3 are mechanically exfoliated on an isotropic SiO_2/Si substrate. **Figure 3**b,d shows ADRDM images of TiS_3 and ZrS_3, respectively. It is obvious that the isotropic substrate does not change with the polarization angle of the linearly polarized incident light. In the other hand, both TiS_3 and ZrS_3 nanoribbons show obvious periodic changes with the polarization angle of the linearly polarized incident light. ADRDM signal can be expressed by the following equation:[35–37]

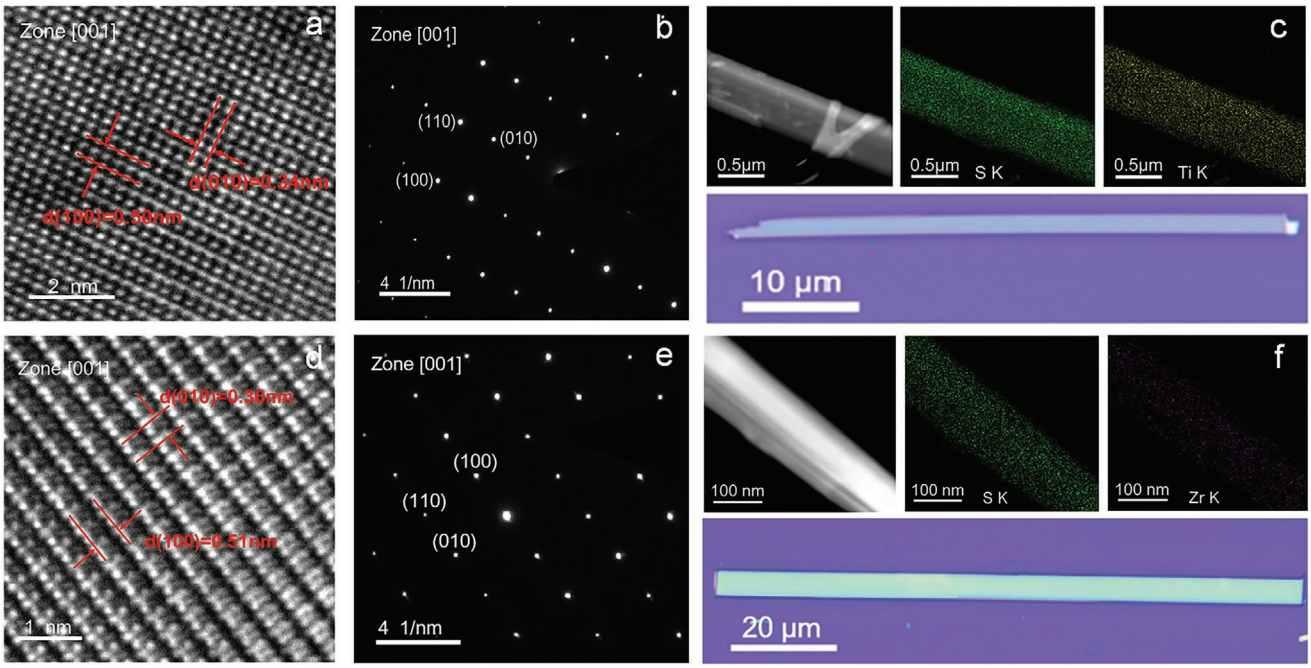

Figure 2. a) HRTEM image of TiS_3. b) SAED pattern of TiS_3. c) Low-magnification TEM image, Energy dispersive X-ray spectroscopy (EDX) mappings of S and Ti, and optical image of TiS_3 nanoribbon. d) HRTEM image of ZrS_3. e) SAED pattern of ZrS_3. f) Low-magnification TEM image, EDX mappings of S and Ti, and optical image of ZrS_3 nanoribbon.

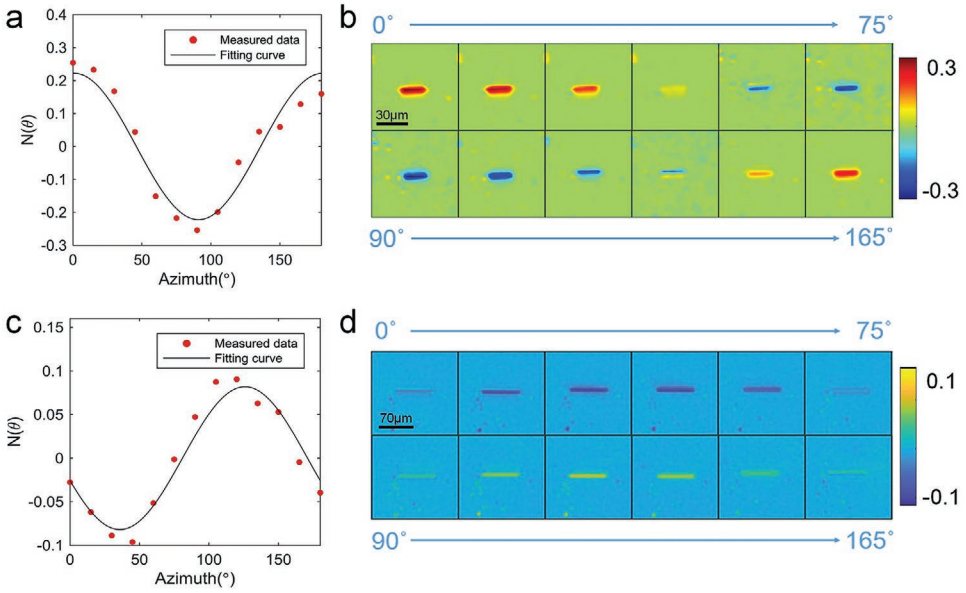

Figure 3. a) ADRDM measured data and fitting curve of TiS_3 nanoribbon. b) ADRDM images of TiS_3 nanoribbon at different rotation angle. c) ADRDM measured data and fitting curve of ZrS_3 nanoribbon. d) ADRDM images of ZrS_3 nanoribbon at different rotation angle.

$$N(\theta) = \frac{|R_a|^2 - |R_b|^2}{|R_a|^2 + |R_b|^2} \cos 2(\theta - \theta_0) \quad (2)$$

where R_a is the reflectivity along the direction of *a*-axis (armchair direction), R_b is the reflectivity along the direction of *b*-axis (zigzag direction), θ is the polarization angle of the linearly polarized incident light, and θ_0 is the initial direction of *b*-axis. Figure 3a,c respectively shows the ADRDM measured data of TiS_3 and ZrS_3 and the curve fitting by equation (2). The measured results in the figures are obtained from the center point data of the measured nanoribbon image at each polarization angle shown in Figure 3b,d. The fitting curve is in good agreement with the variation trend of ADRDM images. This result fully indicates that the reflectivities of TiS_3 and ZrS_3 in different directions are significantly different, which further indicates the anisotropic reflection of those two materials.

After studying the optical anisotropy reflection of TiS_3 and ZrS_3, we further studied their anisotropy refraction by PROM. The anisotropy of 2D materials can be visualized by PROM.[38] Before the measurement, the nanoribbons of TiS_3 and ZrS_3 were mechanically exfoliated on a SiO_2/Si substrate. During the measurement, we adjust the direction of polarization analyzer to be vertical to the linearly polarized incident light and place the previously prepared substrate on the rotating platform. Thus, the PROM is in the orthogonal mode. Images of the TiS_3 and ZrS_3 nanoribbons are recorded with a step of 10° and the dynamic images are shown in Movies S1 and S2, Supporting Information, respectively. The images of representative angle are selected from 0° to 180° by a step of 20°, shown in **Figure 4**a,b. It can be seen in Figure 4a,b that TiS_3 and ZrS_3 nanoribbons have very obvious periodic bright and dark changes with the rotation of the platform, while the substrates are always dark. This phenomenon can indicate the birefringence of TiS_3 and ZrS_3. The cause of this phenomenon is that the substrates are isotropic material, so the refracted light has the same vibration direction as the linearly polarized incident light, so it cannot pass through the polarization analyzer. Darkness is displayed in the field of view, and no matter how the platform is rotated, there is no change in the field of view. However, when the linearly polarized incident light through bifringent materials, the light may be refracted into two components of lights with different vibration directions. So, a part of refracted light can pass through the polarization analyzer and be detected by the charge coupled device. Thus, the birefringence of TiS_3 and ZrS_3 are proved clearly and intuitively.

2.4. Birefringence and Dichroism of TiS_3 and ZrS_3

To study the birefringence and dichroism of TiS_3 and ZrS_3 more systematically and quantitatively, the refractive indices and extinction coefficients of TiS_3 in different directions from theoretical aspects and those of ZrS_3 from both theoretical and experimental aspects were further studied. Birefringence can be expressed by Δn, where Δn is defined as the difference between the refraction indices along in-plane zigzag direction and the armchair direction of TiS_3 and ZrS_3. Similarly, dichroism can be expressed by Δk, where Δk is defined as the difference between the extinction coefficients along in-plane zigzag direction and the armchair direction of TiS_3 and ZrS_3. Theoretically, we used density functional theory (DFT) to calculate the anisotropic refractive indices and extinction coefficients of TiS_3 and ZrS_3. The anisotropy of TiS_3 has been widely studied in previous works. Joshua O. Island and coauthors studied the optical and electrical anisotropy of TiS_3 experimentally.[39] Nikos Papadopoulos and coauthors studied the values of N and K of different directions in-plane of TiS_3 in the wavelength range of 500–700 nm, and based on this, studied the birefringence and dichroism of TiS_3.[13] These previous works all pointed out that TiS_3 has strong anisotropy. Our research on the birefringence

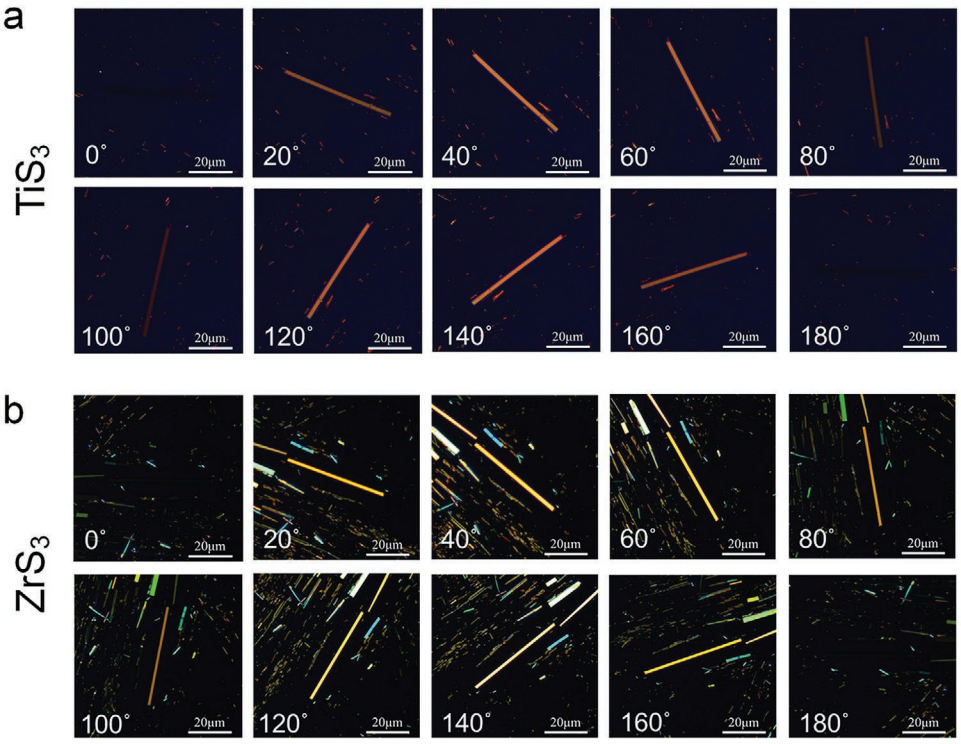

Figure 4. a) PROM images of TiS_3 nanoribbon under polarized light illumination at different rotation angle. b) PROM images of ZrS_3 nanoribbon under polarized light illumination at different rotation angle.

and dichroism of TiS_3 focuses on 200–500 nm, and theoretically calculates the values of N and K in different directions along the plane within this wavelength range, and further obtains the values of birefringence and dichroism of TiS_3. According to our calculation results, it can be seen that TiS_3 has strong anisotropy, which is in good agreement with previous works. The results of the theoretical calculation are shown in Figure S2, Supporting Information. Figure S2a, Supporting Information, shows the refractive indices of TiS_3 in different directions, and n_a is defined as the refractive index along *a*-axis (armchair direction) and n_b is the refractive index along *b*-axis (zigzag direction). As the figure shows, n_a reaches the peak value at the wavelength of 350 nm (the range of calculated wavelength is 200–525 nm), which is $n_a \approx 4$. The peak of n_b appears at 375 nm and the peak value of $n_b \approx 4.2$. Figure S2b, Supporting Information, shows the extinction coefficients of TiS_3 along different directions. We define k_a as the extinction coefficient along *a*-axis and k_b as the extinction coefficient along *b*-axis. As the figure shows, k_a reaches the peak value at the wavelength of 230 nm, which is $k_a \approx 2.3$. The peak of k_b appears at 280 nm, and the peak value of $k_b \approx 2.4$. The change trends of refractive indices and extinction coefficients along different directions of TiS_3 are different. For ZrS_3, calculated refractive indices and extinction coefficients of different direction are shown in **Figure 5**a. It is obviously that n_a reaches the peak value at the wavelength of 250 nm, which is $n_a \approx 3.5$. The peak of n_b appears at approximately the same wavelength (250 nm) and the peak value of $n_b \approx 4$. Figure 5b shows the extinction coefficients of ZrS_3 along different directions. It is obvious that the peak value of k_a is $k_a \approx 2.2$ at the wavelength of 250 nm. In the other hand, the peak of k_b appears at 200 nm, and the peak value of $k_b \approx 2.3$. The change trends of refractive indices and extinction coefficients along different directions of ZrS_3 are also different. This phenomenon indicates that both TiS_3 and ZrS_3 have obvious optical anisotropies including birefringence and dichroism. Furthermore, according to the above definitions of birefringence Δn and dichroism Δk, we define that: $\Delta n = n_a - n_b$, $\Delta k = k_a - k_b$. Figure S2c, Supporting Information, and Figure 5c show the birefringence Δn and dichroism Δk of TiS_3 and ZrS_3, respectively. As the figures show, it is obvious that both TiS_3 and ZrS_3 display a giant birefringence and dichroism. These results can also prove that both TiS_3 and ZrS_3 have obvious optical anisotropies.

In order to further study the birefringence and dichroism of quasi-1D TMTC and verify the accuracy of theoretical calculation, we measured the refractive indices and extinction coefficients of bulk ZrS_3 along different directions experimentally by Mueller matrix SE. At present, SE measurements is often used to study the optical properties of thin film materials or large-size bulk materials.[40–42] Schematic image of Mueller matrix SE measurements is shown in Figure S3, Supporting Information. The SE measures the complete Mueller matrix of the sample based on the dual-rotating compensator principle.[43] In the SE measurements, the linearly polarized light is generated by a linear polarizer and modulated by a rotating compensator. The continuously modulated polarized light is illuminated on the bulk ZrS_3 sample and then reflected after incorporating the optical information of the sample. The polarized light reflected from the sample is further demodulated by a second rotating compensator following by another linear polarizer (usually known as the analyzer), and finally detected by a spectrometer.

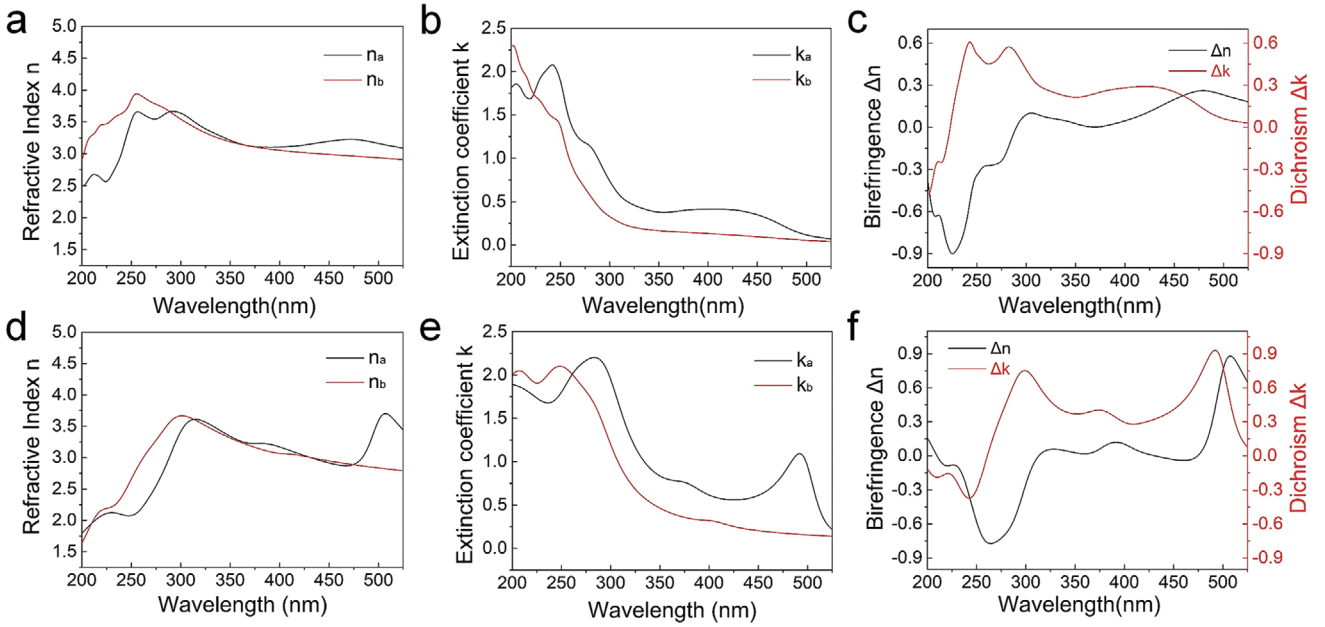

Figure 5. a) Calculated refractive index of ZrS_3 along *a*-axis and *b*-axis. b) Calculated extinction coefficient of ZrS_3 along *a*-axis and *b*-axis. c) Calculated birefringence and dichroism of ZrS_3. d) Refractive index of ZrS_3 along *a*-axis and *b*-axis measured by SE. e) Extinction coefficient of ZrS_3 along *a*-axis and *b*-axis measured by SE. f) Birefringence and dichroism of ZrS_3 measured by SE.

The first and the second compensators are rotated synchronously by hollow servo motors with an angular velocity ratio of 5 : 3. By detecting and analyzing the modulated light intensity, the Mueller matrix of the sample can be obtained, which contains abundant information, especially including the optical anisotropy, about the sample. The synchronization controller and data acquisition system are connected with a computer, which is also responsible for the data processing. The measurement can be performed at different incident angles among the range of 45–90° and azimuthal angles among the range of 0–360° by rotating the two arms of the SE and the sample stage with six degrees of freedom, respectively. By performing ellipsometric analysis, the optical information such as anisotropic refractive indices and extinction coefficients of the sample can be extracted from the measured Mueller matrix.[43] Figure 5d shows the refractive indices n_a and n_b of ZrS_3 measured by SE measurements along *a*-axis and *b*-axis. The measured refractive index n_a of ZrS_3 along *a*-axis reached its peak value at the wavelength of ≈320 nm, and the peak value is n_a≈3.7. The measured refractive index n_b reaches a peak value at the wavelength of ≈280 nm, and the peak value is n_b≈3.8. By comparing the experimental results with the theoretical calculation results, it is obvious that the peak values of the refractive indices of ZrS_3 along different directions and the change trend of the refractive index in the measured wavelength are in good agreement with the theoretical calculation. In terms of the peak position, the measured peak position has a red shift to a certain extent compared with the theoretically calculated peak position. This phenomenon might be caused by the selection of the calculation model, the internal defects of the material, and the errors in the measurements. However, this redshift is small, and the peak value and the change tendency of measured refractive index of ZrS_3 have good agreement with theoretical calculation results in the range of calculated wavelength. The results show the value of refractive index of bulk ZrS_3 under different wavelength along *a*-axis and *b*-axis, and further effectively illustrate that ZrS_3 has obvious optical anisotropy. The extinction coefficients k_a and k_b of bulk ZrS_3 measured by SE along *a*-axis and *b*-axis are shown in Figure 5e. As the figure shows, k_a reaches the peak value at the wavelength of 300 nm, which is $k_a \approx 2.3$. The peak of k_b appears at 260 nm, and the peak value of $k_b \approx$ 2.1. By comparing the calculation results in Figure 5b, the measurement results of extinction coefficients of ZrS_3 are basically the same as the theoretical calculation results in terms of peak value and change trend, and the peak position is also redshifted. This comparison result is consistent with the comparison result of the refractive indices of ZrS_3 along different directions mentioned above. This result indicates that the cause of this redshift is the same as the cause of refractive index redshift described above. Figure 5f shows the experimentally measured birefringence Δn and dichroism Δk of ZrS_3, a similar result with Figure 5c. This result intuitively shows that measured refractive indices and extinction coefficients in the experiments are reliable. Furthermore, we provide theoretical and experimental comparison of birefringence and dichroism for ZrS_3 in Figure S4, Supporting Information. As can be seen from Figure S4, Supporting Information, the experimental and theoretical data trends are in good agreement, but there are some differences in the numerical value of high wave strength. We believe that these differences mainly come from the defects of materials and the errors of instruments. Finally, some typical data of TiS_3 and ZrS_3 are extracted and shown in **Table 1**. To conclusion, both refractive indices and extinction coefficients of bulk ZrS_3 along *a*-axis and *b*-axis have obviously different peak values and change trends. The measured data and theoretical calculation data can match with each other. This result illustrates that TiS_3

Table 1. Calculated birefringence and dichroism of TiS_3, ZrS_3 and measured birefringence and dichroism of ZrS_3.

Material		Wavelength [nm]	n_a	n_b	k_a	k_b	Δn	Δk
TiS_3	Theoretical	200	1.79	2.15	2.21	2.19	–0.36	0.03
	Results	300	3.39	3.97	2.20	1.91	–0.58	0.29
		400	3.62	3.94	0.70	0.54	–0.32	0.16
		500	3.37	3.62	0.86	0.20	–0.25	0.66
ZrS_3	Theoretical	200	2.50	2.90	1.82	2.30	–0.40	–0.48
	Results	300	3.63	3.54	0.73	0.32	0.09	0.41
		400	3.10	3.06	0.41	0.13	0.04	0.28
		500	3.16	2.94	0.11	0.05	0.22	0.06
ZrS_3	Experimental	200	1.79	1.63	1.89	2.00	0.16	–0.11
	Results	300	3.42	3.67	1.95	1.20	–0.25	0.75
		400	3.17	3.07	0.62	0.32	0.10	0.30
		500	3.59	2.83	0.94	0.16	0.76	0.78

and ZrS_3 have obvious anisotropy, and demonstrates that using SE measurements to study anisotropic refractive indices and extinction coefficients of quasi-1D structure material such as ZrS_3 along different directions is a feasible method.

3. Conclusion

In conclusion, we systematically study the birefringence and dichroism of quasi-1D TMTC materials TiS_3 and ZrS_3. First, the crystal structure, energy band, and anisotropic optical absorption of TiS_3 and ZrS_3 are theoretically calculated, respectively. Then, anisotropic refraction and anisotropic reflection of the two materials are investigated experimentally using PROM and ADRDM. Finally, we calculate the birefringence Δn and dichroism Δk of TiS_3 and ZrS_3 by DFT, and for the first time measure the refractive indices and extinction coefficients of ZrS_3 along different directions experimentally by SE measurements, and obtain the birefringence Δn and dichroism Δk. The results of SE measurements are in good agreement with the theoretical calculation results, which obviously indicate that ZrS_3 has strong optical anisotropy and indicates that it is a feasible way to measure the anisotropic refractive indices and extinction coefficients of quasi-1D TMTC bulk materials by SE measurements. This work provides basic optical anisotropy information such as birefringence Δn and dichroism Δk of two kinds of quasi-1D TMTC materials TiS_3 and ZrS_3, which lays a foundation for the further study of optoelectronic applications based on these two materials in the future, also provides a feasible method for the study of birefringence and dichroism of other materials.

Supporting Information

Supporting Information is available from the Wiley Online Library or from the author.

Acknowledgements

This work was financially supported by the National Key Research and Development Program of China (Grant No. 2017YFA0207500), the National Natural Science Foundation of China (Grant No. 62004193, 12004375, 51727809, 51805193), the Strategic Priority Research Program of Chinese Academy of Sciences (XDB43000000), and Beijing National Laboratory for Molecular Sciences (BNLMS201908).

Conflict of Interest

The authors declare no conflict of interest.

Data Availability Statement

Research data are not shared.

Keywords

birefringence, dichroism, spectrometric ellipsometry, TMTC material

Received: January 24, 2021
Revised: March 29, 2021
Published online: April 22, 2021

[1] M. F. Weber, C. A. Stover, L. R. Gilbert, T. J. Nevitt, A. J. Ouderkirk, *Science* **2000**, *287*, 2451.
[2] L. H. Nicholls, F. J. Rodríguez-Fortuño, M. E. Nasir, R. M. Córdova-Castro, N. Olivier, G. A. Wurtz, A. V. Zayats, *Nat. Photonics* **2017**, *11*, 628.
[3] S. Huang, Y. Tatsumi, X. Ling, H. Guo, Z. Wang, G. Watson, A. A. Puretzky, D. B. Geohegan, J. Kong, J. Li, *ACS Nano* **2016**, *10*, 8964.
[4] M. A. Kats, P. Genevet, G. Aoust, N. Yu, R. Blanchard, F. Aieta, Z. Gaburro, F. Capasso, *Proc. Natl. Acad. Sci. USA* **2012**, *109*, 12364.
[5] M. Long, A. Gao, P. Wang, H. Xia, C. Ott, C. Pan, Y. Fu, E. Liu, X. Chen, W. Lu, *Sci. Adv.* **2017**, *3*, e1700589.
[6] Y. Yang, S.-C. Liu, Y. Wang, M. Long, C.-M. Dai, S. Chen, B. Zhang, Z. Sun, Z. Sun, C. Hu, S. Zhang, L. Tong, G. Zhang, D.-J. Xue, J.-S. Hu, *Adv. Opt. Mater.* **2019**, *7*, 1801311.
[7] Q. Cui, A. Lipatov, J. S. Wilt, M. Z. Bellus, X. C. Zeng, J. Wu, A. Sinitskii, H. Zhao, *ACS Appl. Mater. Interfaces* **2016**, *8*, 18334.

[8] I. Ferrer, J. Ares, J. Clamagirand, M. Barawi, C. Sánchez, *Thin Solid Films* **2013**, *535*, 398.
[9] I. Ferrer, M. Maciá, V. Carcelén, J. Ares, C. Sánchez, *Energy Procedia* **2012**, *22*, 48.
[10] S. J. Gilbert, A. Lipatov, A. J. Yost, M. J. Loes, A. Sinitskii, P. A. Dowben, *Appl. Phys. Lett.* **2019**, *114*, 101604.
[11] J. O. Island, M. Buscema, M. Barawi, J. M. Clamagirand, J. R. Ares, C. Sánchez, I. J. Ferrer, G. A. Steele, H. S. van der Zant, A. Castellanos-Gomez, *Adv. Opt. Mater.* **2014**, *2*, 641.
[12] A. Lipatov, M. J. Loes, H. Lu, J. Dai, P. Patoka, N. S. Vorobeva, D. S. Muratov, G. Ulrich, B. Kästner, A. Hoehl, *ACS Nano* **2018**, *12*, 12713.
[13] N. Papadopoulos, R. Frisenda, R. Biele, E. Flores, J. R. Ares, C. Sánchez, H. S. van der Zant, I. J. Ferrer, R. D'Agosta, A. Castellanos-Gomez, *Nanoscale* **2018**, *10*, 12424.
[14] A. Pant, E. Torun, B. Chen, S. Bhat, X. Fan, K. Wu, D. P. Wright, F. M. Peeters, E. Soignard, H. Sahin, *Nanoscale* **2016**, *8*, 16259.
[15] X. Wang, K. Wu, M. Blei, Y. Wang, L. Pan, K. Zhao, C. Shan, M. Lei, Y. Cui, B. Chen, *Adv. Electron. Mater.* **2019**, *5*, 1900419.
[16] S. Liu, W. Xiao, M. Zhong, L. Pan, X. Wang, H.-X. Deng, J. Liu, J. Li, Z. Wei, *Nanotechnology* **2018**, *29*, 184002.
[17] J. O. Island, M. Barawi, R. Biele, A. Almazán, J. M. Clamagirand, J. R. Ares, C. Sánchez, H. S. Van Der Zant, J. V. Álvarez, R. D'Agosta, *Adv. Mater.* **2015**, *27*, 2595.
[18] A. Lipatov, P. M. Wilson, M. Shekhirev, J. D. Teeter, R. Netusil, A. Sinitskii, *Nanoscale* **2015**, *7*, 12291.
[19] A. J. Molina-Mendoza, J. O. Island, W. S. Paz, J. M. Clamagirand, J. R. Ares, E. Flores, F. Leardini, C. Sánchez, N. Agraït, G. Rubio-Bollinger, *Adv. Funct. Mater.* **2017**, *27*, 1605647.
[20] Y. Niu, R. Frisenda, E. Flores, J. R. Ares, W. Jiao, D. Perez de Lara, C. Sánchez, R. Wang, I. J. Ferrer, A. Castellanos-Gomez, *Adv. Opt. Mater.* **2018**, *6*, 1800351.
[21] M. Randle, A. Lipatov, A. Kumar, C.-P. Kwan, J. Nathawat, B. Barut, S. Yin, K. He, N. Arabchigavkani, R. Dixit, *ACS Nano* **2018**, *13*, 803.
[22] M. Talib, R. Tabassum, Abid, S. S. Islam, P. Mishra, *ACS Omega* **2019**, *4*, 6180.
[23] S. J. Gilbert, H. Yi, J. S. Chen, A. J. Yost, A. Dhingra, J. Abourahma, A. Lipatov, J. Avila, T. Komesu, A. Sinitskii, M. C. Asensio, P. A. Dowben, *ACS Appl. Mater. Interfaces* **2020**, *12*, 40525.
[24] S. Furuseth, L. Brattås, A. Kjekshus, A. Andresen, P. Fischer, *Acta Chem. Scand.* **1975**, *29*, 623.
[25] K. Momma, F. Izumi, *J. Appl. Crystallogr.* **2008**, *41*, 653.
[26] J. Heyd, J. E. Peralta, G. E. Scuseria, R. L. Martin, *J. Chem. Phys.* **2005**, *123*, 174101.
[27] J. Wu, D. Wang, H. Liu, W.-M. Lau, L.-M. Liu, *RSC Adv.* **2015**, *5*, 21455.
[28] G. Kresse, J. Furthmüller, *Phys. Rev. B* **1996**, *54*, 11169.
[29] W. Kohn, L. J. Sham, *Phys. Rev.* **1965**, *140*, A1133.
[30] G. Kresse, J. Hafner, *Phys. Rev. B: Condens. Matter Mater. Phys.* **1993**, *47*, 558.
[31] P. E. Blochl, *Phys. Rev. B: Condens. Matter Mater. Phys.* **1994**, *50*, 17953.
[32] J. P. Perdew, K. Burke, M. Ernzerhof, *Phys. Rev. Lett.* **1996**, *77*, 3865.
[33] P. E. Blöchl, *Phys. Rev. B* **1994**, *50*, 17953.
[34] H. J. Monkhorst, J. D. Pack, *Phys. Rev. B* **1976**, *13*, 5188.
[35] S. Yang, Y. Yang, M. Wu, C. Hu, W. Shen, Y. Gong, L. Huang, C. Jiang, Y. Zhang, P. M. Ajayan, *Adv. Funct. Mater.* **2018**, *28*, 1707379.
[36] Y. Yang, S. C. Liu, X. Wang, Z. Li, Y. Zhang, G. Zhang, D. J. Xue, J. S. Hu, *Adv. Funct. Mater.* **2019**, *29*, 1900411.
[37] J. Tao, W. Shen, S. Wu, L. Liu, Z. Feng, C. Wang, C. Hu, P. Yao, H. Zhang, W. Pang, *ACS Nano* **2015**, *9*, 11362.
[38] H. Yang, H. Jussila, A. Autere, H.-P. Komsa, G. Ye, X. Chen, T. Hasan, Z. Sun, *ACS Photonics* **2017**, *4*, 3023.
[39] J. O. Island, R. Biele, M. Barawi, J. M. Clamagirand, J. R. Ares, C. Sanchez, H. S. van der Zant, I. J. Ferrer, R. D'Agosta, A. Castellanos-Gomez, *Sci. Rep.* **2016**, *6*, 22214.
[40] B. Song, H. Gu, S. Zhu, H. Jiang, X. Chen, C. Zhang, S. Liu, *Appl. Surf. Sci.* **2018**, *439*, 1079.
[41] M. Fang, Z. Wang, H. Gu, M. Tong, B. Song, X. Xie, T. Zhou, X. Chen, H. Jiang, T. Jiang, S. Liu, *Appl. Surf. Sci.* **2020**, *509*, 144822.
[42] S. Niu, G. Joe, H. Zhao, Y. Zhou, T. Orvis, H. Huyan, J. Salman, K. Mahalingam, B. Urwin, J. Wu, Y. Liu, T. E. Tiwald, S. B. Cronin, B. M. Howe, M. Mecklenburg, R. Haiges, D. J. Singh, H. Wang, M. A. Kats, J. Ravichandran, *Nat. Photonics* **2018**, *12*, 392.
[43] H. Gu, X. Chen, H. Jiang, C. Zhang, S. Liu, *J. Opt.* **2016**, *18*, 025702.

NANO MICRO small

Supporting Information

for *Small,* DOI: 10.1002/smll.202100457

Birefringence and Dichroism in Quasi-1D Transition Metal Trichalcogenides: Direct Experimental Investigation

Shijun Hou, Zhengfeng Guo, Juehan Yang, Yue-Yang Liu, Wanfu Shen, Chunguang Hu, Shiyuan Liu, Honggang Gu, and Zhongming Wei**

Supporting Information

Birefringence and Dichroism in Quasi-One-Dimensional Transition Metal Trichalcogenides: Direct Experimental Investigation

Shijun Hou, Zhengfeng Guo, Juehan Yang, Yue-Yang Liu, Wanfu Shen, Chunguang Hu, Shiyuan Liu, Honggang Gu, and Zhongming Wei**

S. Hou, Dr. J. Yang, Dr. Y.-Y Liu, Prof. Z. Wei
State Key Laboratory of Superlattices and Microstructures, Institute of Semiconductors, Chinese Academy of Sciences & Center of Materials Science and Optoelectronics Engineering, University of Chinese Academy of Sciences, Beijing 100083, China.
E-mail: zmwei@semi.ac.cn

Z. Guo, Prof. S. Liu, Dr. H. Gu
State Key Laboratory of Digital Manufacturing Equipment and Technology, Huazhong University of Science and Technology, Wuhan 430074, China.
E-mail: hongganggu@hust.edu.cn

Dr. W. Shen, Prof. C. Hu
State Key Laboratory of Precision Measuring Technology and Instruments, Tianjin University Tianjin 300072, China.

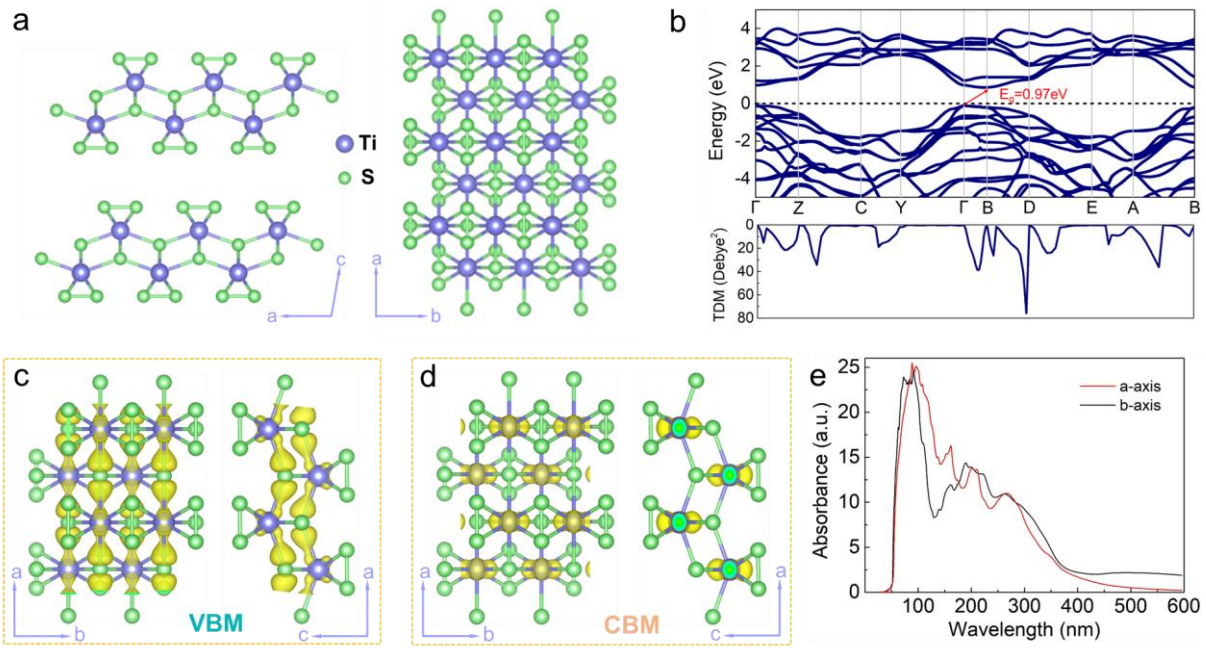

Figure S1. (a) Crystal structure of TiS_3. (b) Calculated band structure and transition dipole moment of TiS_3. (c) Calculated Partial charge density (PCD) of valence band maximum (VBM) in TiS_3. (d) Calculated PCD of conduction band minimum (CBM) in TiS_3. (e) Calculated anisotropy optical absorbance along the a-axis and b-axis of TiS_3.

Movie S1. Dynamic PROM images of TiS_3 nanoribbon in the orthogonal mode.

Movie S2. Dynamic PROM images of ZrS_3 nanoribbon in the orthogonal mode.

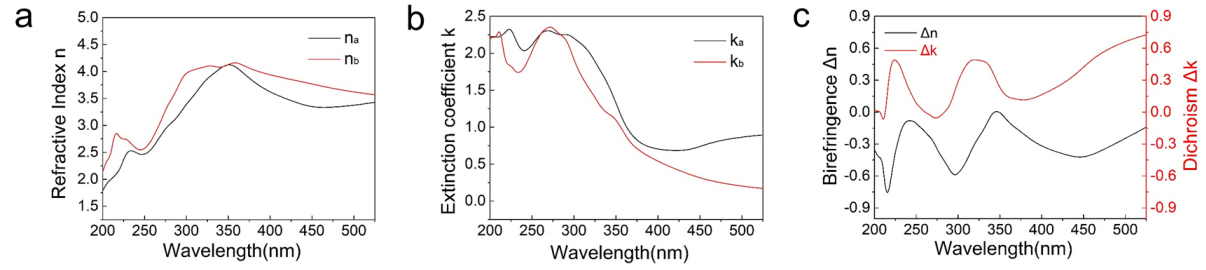

Figure S2. (a) Calculated refractive index of TiS_3 along a-axis and b-axis. (b) Calculated extinction coefficient of TiS_3 along a-axis and b-axis. (c) Calculated birefringence and dichroism of TiS_3.

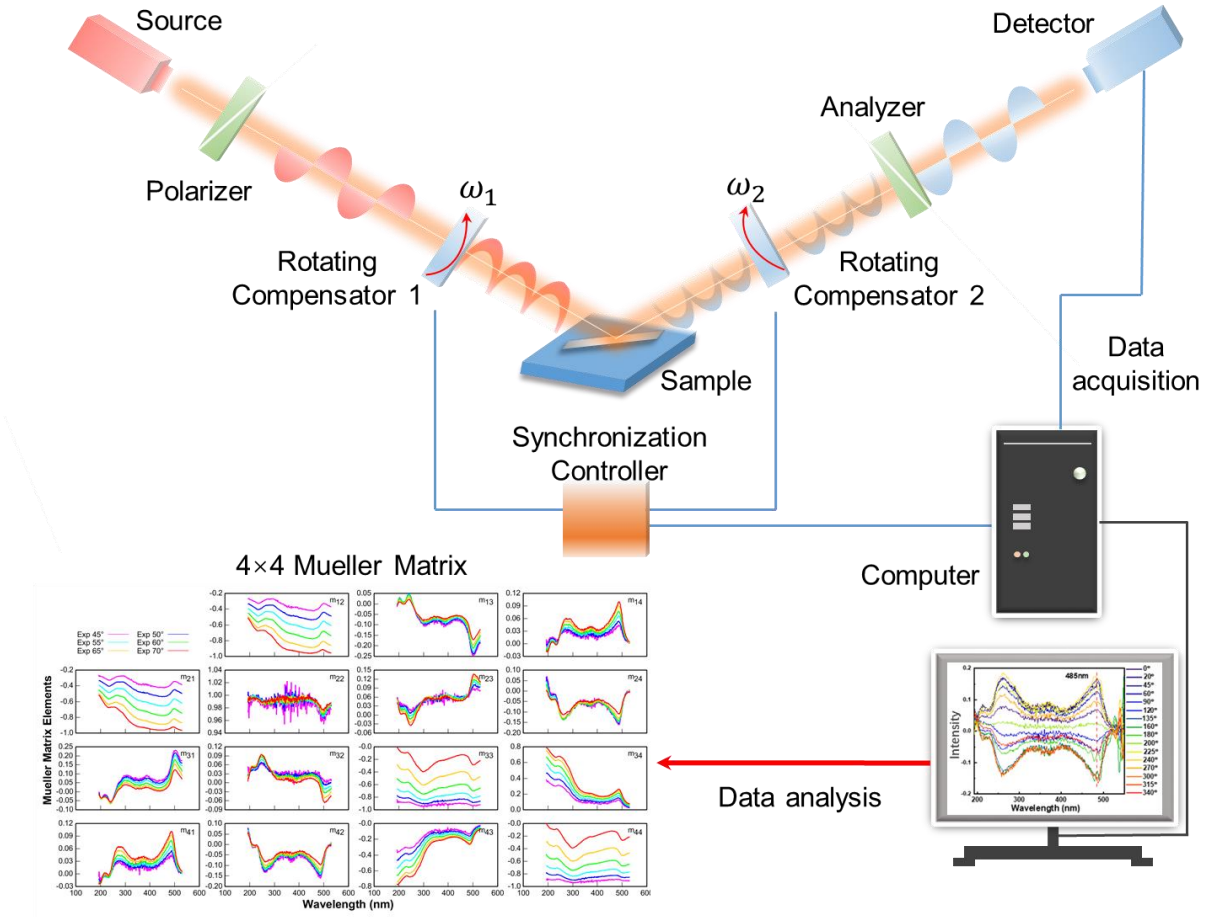

Figure S3. Schematic image of Mueller matrix spectrometric ellipsometry (SE) measurements.

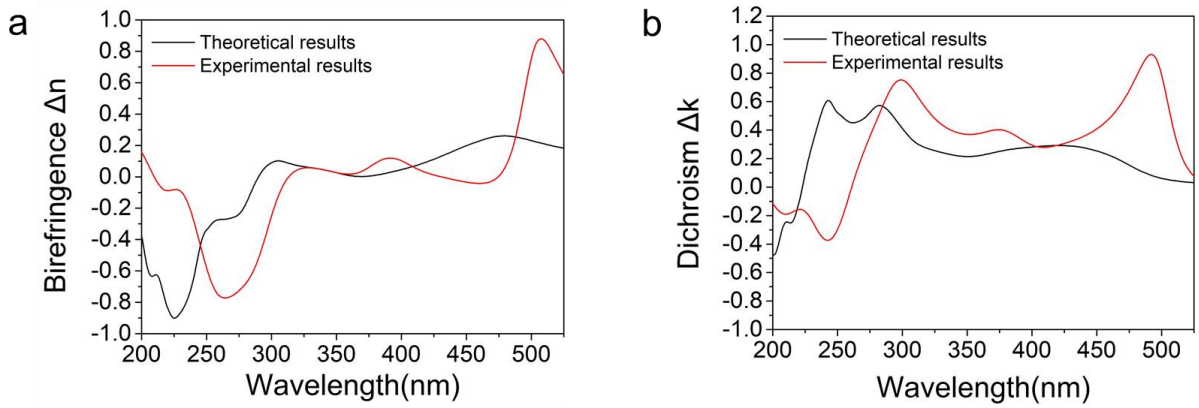

Figure S4. Theoretical and experimental comparison of birefringence and dichroism in ZrS_3.